

Interactions of Fundamental Mie Modes with Thin Epsilon-near-Zero Substrates

Mohammad Karimi,* Kashif Masud Awan, Yaswant Vaddi, Rasoul Alaei, Jeremy Upham, M. Zahirul Alam,* and Robert W. Boyd



Cite This: <https://doi.org/10.1021/acs.nanolett.3c03301>



Read Online

ACCESS |



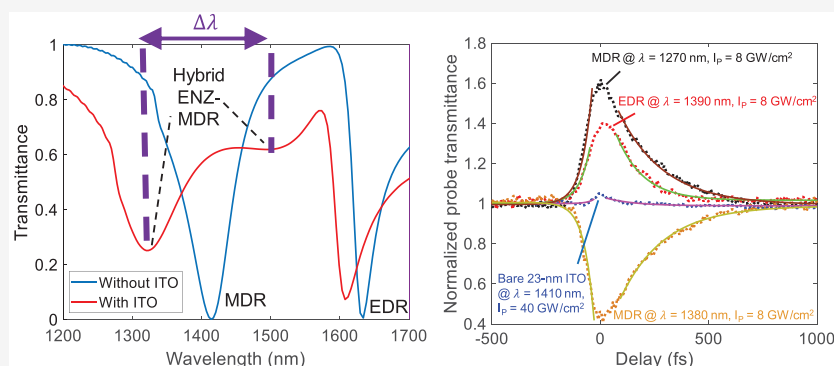
Metrics & More



Article Recommendations



Supporting Information



ABSTRACT: Extensive research has focused on Mie modes in dielectric nanoresonators, enabling the creation of thin optical devices surpassing their bulk counterparts. This study investigates the interactions between two fundamental Mie modes, electric and magnetic dipoles, and the epsilon-near-zero (ENZ) mode. Analytical, simulation, and experimental analyses reveal that the presence of the ENZ substrate significantly modifies these modes despite a large size mismatch. Electric and magnetic dipole modes, both with ~ 12 THz line widths, exhibit 21 and 26 THz anticrossings, respectively, when coupled to the ENZ mode, indicating strong coupling. We also demonstrate that this strongly coupled system yields notably large subpicosecond nonlinear responses. Our results establish a solid foundation for designing functional, nonlinear, dynamic dielectric metasurfaces with ENZ materials.

KEYWORDS: Nonlinear Optics, Epsilon-near-Zero, Metasurface, Nano-optics

Dielectric nanoantennas, constructed from materials with high refractive indices and low loss compared to plasmonic counterparts, serve as the building blocks for the next generation of nanophotonic devices.¹ Unlike plasmonic nanoantennas, they easily integrate into existing CMOS fabrication lines² and, even with simple geometries, support multiple optical resonances, including electric and magnetic dipoles and quadrupoles, referred to as Mie modes.³ The availability of multiple resonant modes in the dielectric nanoantennas allows for tailoring near-field and far-field properties of light.^{4–22} In a parallel vein, thin layers of ENZ materials have distinctive linear and nonlinear optical properties arising from a nearly zero real part of permittivity within specific wavelength ranges.²³ Notably, materials such as indium tin oxide (ITO) and aluminum-doped zinc oxide (AZO) have been extensively explored for their large nonlinear responses.^{24,25}

In this work, we investigate how the Mie resonances of the dielectric nanoantenna couple with the ENZ mode of a thin ITO substrate. An ENZ mode is an inherently dark mode with a largely enhanced electric field inside a very thin ENZ layer

sandwiched between two dielectrics.²⁶ Extensive research has been conducted on the interaction between the modes of plasmonic nanostructures and the ENZ mode of various near-zero-permittivity materials, including transparent conducting oxides,^{27,28} semiconductors,²⁹ and phonon-based ENZ materials.³⁰ Plasmonic systems often exhibit pronounced losses, which need to be addressed. Additionally, achieving higher-order modes in these systems necessitates intricate engineering efforts to shape the antennas, adding an additional layer of complexity to the design process.³¹ In Mie resonances, unlike plasmonic resonances, the mode is typically concentrated within the dielectric material rather than along the surfaces; therefore, the opportunity for strong modal overlap with the ENZ mode of a nearby structure is expected to be smaller.

Received: August 31, 2023

Revised: November 23, 2023

Accepted: November 27, 2023

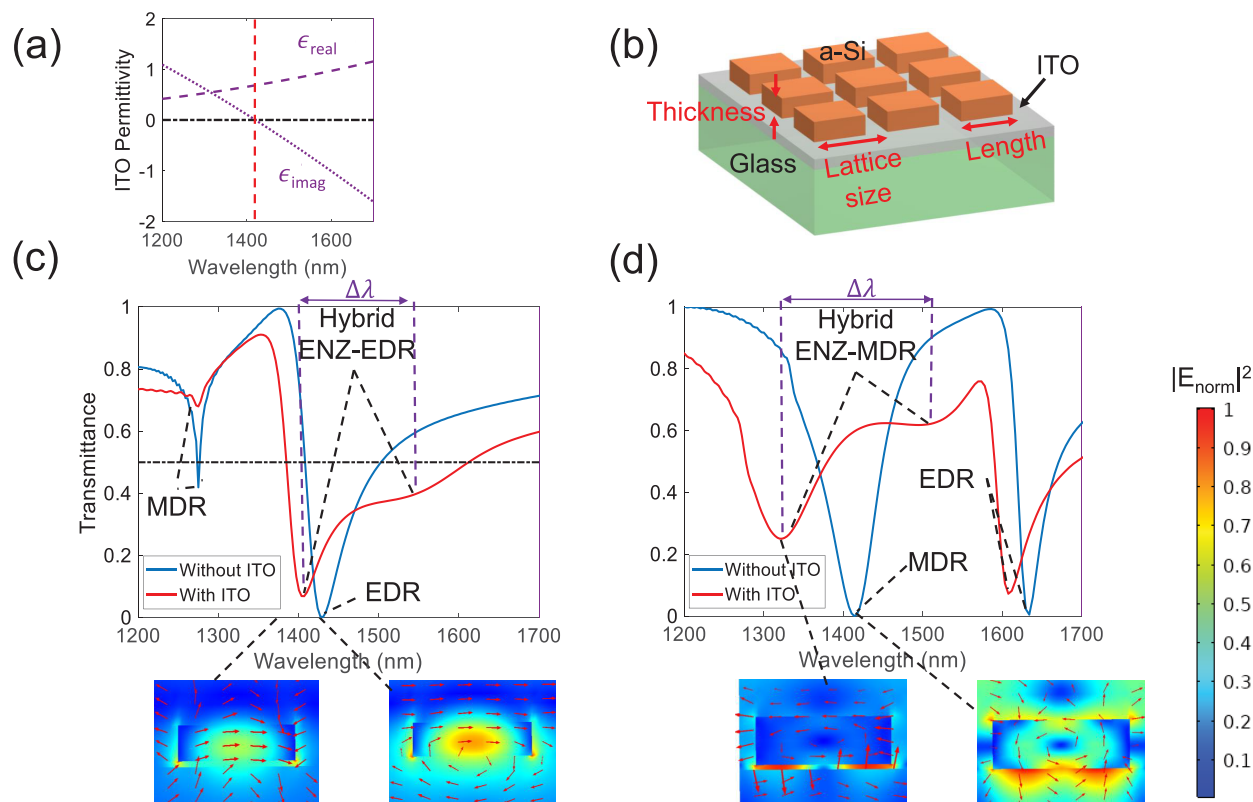


Figure 1. (a) The real and imaginary parts of the permittivity of the ITO sample taken from the ellipsometry data; the red dashed line specifies that 1410 nm is the zero crossing point. (b) The schematics of the a-Si metasurface on ITO on glass. (c, d) Comparison of the transmittance of the metasurfaces over the glass and over ITO for observing the interaction of the (c) electric dipole resonance (EDR) and (d) magnetic dipole resonance (MDR) with the ENZ mode. The length, width, and thickness of the antennas and the lattice constant in the figure are 560, 500, 140, and 850 nm, respectively, for part c and 650, 650, 210, and 810 nm, respectively, for part d. The parameter $\Delta\lambda$ indicates the amount of anticrossing that occurs due to the strong coupling effect, and it is around 140 nm for the EDR case and around 200 nm for the MDR case. The insets show the electric field amplitude distribution and direction around the antennas for the different resonance modes specified in the transmittance plots.

However, we show that even for a simple dielectric nanoantenna geometry, the field enhancement of Mie modes is sufficient to achieve strong coupling with the ENZ mode. We experimentally and theoretically demonstrate that the two fundamental Mie modes (electric and magnetic dipole resonances) of silicon dielectric antennas can strongly couple with the ENZ mode of a 23 nm-thick ITO substrate. Furthermore, using simple pump–probe measurements, we demonstrate strongly enhanced transmission modulation of these structures in comparison to bare ITO. This suggests that the metasurface composed of dielectric nanoantennas and ENZ thin films has significant potential for nonlinear optical applications, at least as significant and perhaps more varied than their plasmonic counterparts.

In general, the resonance wavelength of a Mie mode is a complicated function of the geometric and material properties of the dielectric nanoantenna. We selected cuboid antenna shapes since the three geometric parameters length, width, and height allow sufficient freedom to investigate the interaction between one fundamental dipole resonance (either electric or magnetic) and the ENZ mode while keeping the other dipole resonance spectrally separate from the ENZ resonance condition.³² Figures 1a and b demonstrate the permittivity of the ITO substrate we used and a schematic of the device with and without ITO, respectively. The ENZ mode resonance, as discussed in section 1 of the Supporting Information, is near the wavelength where the real part of the permittivity crosses

from positive to negative, that is, the wavelength at which Mie resonances could couple to the ENZ mode. In this work, we focus on the electric dipole resonance (EDR) and the magnetic dipole resonance (MDR) of the antennas. Higher-order modes, such as quadrupole, likely respond similarly but will be the subject of subsequent research. We designed two groups of metasurfaces, each specifically engineered to align either the EDR or the MDR with the wavelength of the ENZ mode, while ensuring all other resonance modes remain at least two line widths distant from the ENZ wavelength. To design the metasurfaces, we swept over different dimensions of the single antennas and the lattice constant over the glass in our simulations using Comsol Multiphysics while tracking the resonance wavelength and mode of each of the Mie resonances. We then found the dimensions that set the resonances to the ENZ mode's central wavelength, added the ITO layer as the substrate, and compared the results in the presence and absence of ITO. Figure 1 demonstrates the effect of a 23 nm layer of ITO as the substrate on the transmittance of one of our EDR samples and one of our MDR samples, respectively. The length, width, and thickness of the antennas and the lattice constant in Figure 1 are 560, 500, 140, and 850 nm, respectively, for the EDR case and 650, 650, 210, and 810 nm, respectively, for the MDR case. In both cases, the presence of ITO splits the Mie resonance into two hybrid modes: one at a shorter wavelength and one at a longer wavelength than the resonance wavelength of the same metasurfaces on glass; we

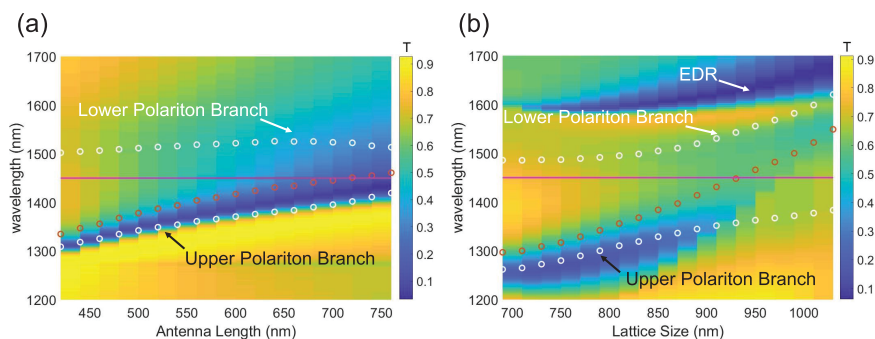


Figure 2. Comparison of analytical derivation and numerical simulation of hybridized mode splitting. To show tuning of (a) the EDR and (b) the MDR across the ENZ mode, transmittance spectra for different antenna lengths or lattice sizes, respectively, were simulated in Comsol Multiphysics. The red circles are the position of the EDR and MDR in parts a and b, respectively, with the antennas without ITO derived from the simulation results. The white circles indicate the positions of the upper and lower polariton branches predicted by the analytical solution.

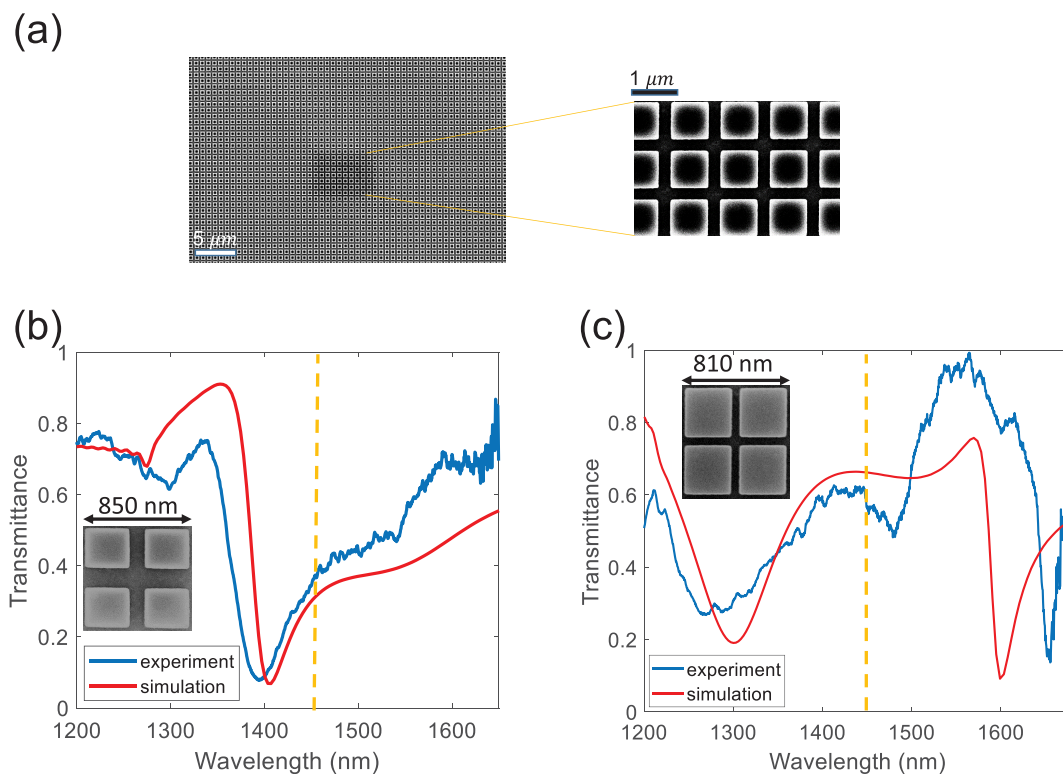


Figure 3. (a) SEM image of one of the fabricated devices. (b, c) Comparison of the transmittance in simulation and experiment of one representative EDR sample (b) and one representative MDR sample (c). The vertical dashed line shows the central wavelength of the ENZ mode. The SEM images in the insets show 4 unit cells of the metasurface for which the experimental data is shown. The dimensions of the samples were the same as those used in Figure 1. The orange dashed lines specify the central wavelength of the ENZ mode derived by solving the wave equation as explained in the Supporting Information.

call them the lower polariton branch and the upper polariton branch, respectively, for the remainder of the manuscript. Note that the lower polariton branch exhibits a smaller dip in transmittance than the upper polariton branch, which can be attributed to the non-negligible loss of ITO. A similar asymmetry in the depth of the transmission resonances has been reported before.^{33,34} The appearance of these hybrid modes is the main sign of coupling between the fundamental Mie modes and the ENZ mode.³⁵ The spectral separation of the hybrid modes, $\Delta\lambda$, is proportional to the strength of coupling, and the system is said to be in a strong coupling regime if the spectral separation is larger than the line width of the fundamental Mie mode in the absence of ITO.³⁵ These simulations predict hybridized mode splitting larger than the

FWHM line width of the Mie resonances without the ITO substrate, suggesting that the systems are in strong coupling regimes.

The field distributions of the EDR and MDR are distinguishable inside and in the vicinity of the nanoantennas at the resonance wavelength.^{32,36} The insets in Figure 1c and d show the electric field intensities and vectorial distributions at the EDR and MDR without the ITO thin film as well as the higher polariton branch of each when this ENZ substrate is included. At the EDR, the electric field concentrates within the center of the nanoantenna, with the polarization determined by the incident field. At the MDR, the electric field vectors circle inside the antenna such that the curl of the electric field points in the direction of the magnetic dipole. When introducing a

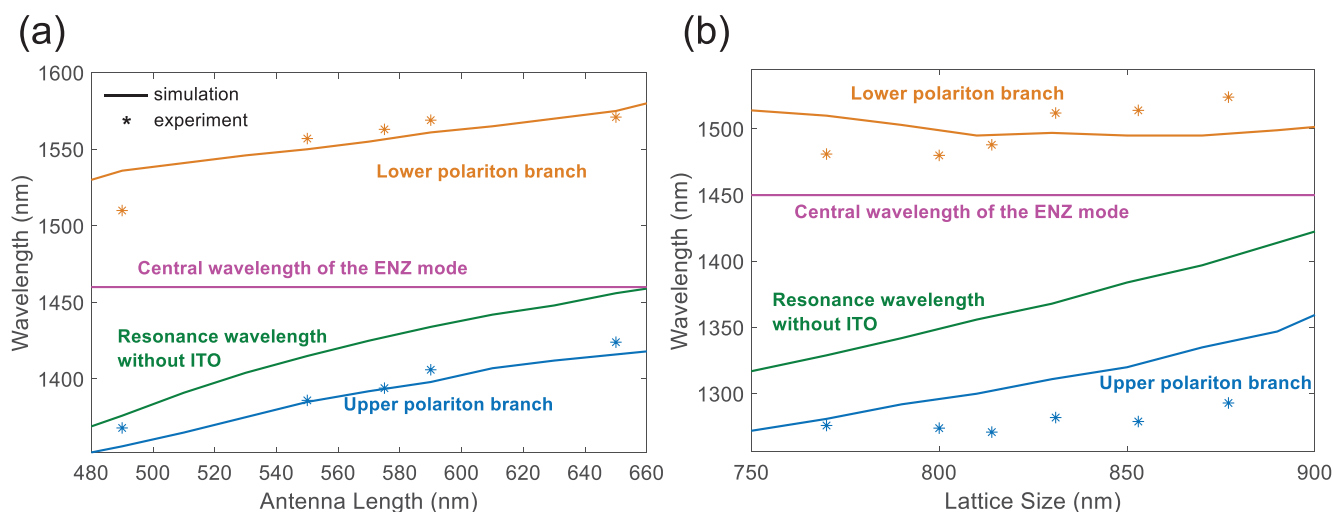


Figure 4. Positions of different resonances in the wavelength domain for (a) the EDR sample for different antenna lengths and (b) the MDR sample for different lattice sizes.

thin ITO layer as the substrate, the upper polariton resonances show that a visibly significant portion of the electric field within the antennas penetrates the ITO layer due to strong coupling for both resonances.

To investigate the strongly coupled system in more detail, we simulated the transmittance of the metasurfaces with different dimensions for the EDR and MDR samples using Comsol Multiphysics. Sweeping the dimensions such that one Mie resonance crossed the ENZ mode revealed the anticrossing of the hybridized modes in the transmittance. Figures 2a and b show the simulated transmittance at different wavelengths for EDR and MDR samples, respectively, as functions of the length of the antennas for the EDR samples and the size of the lattice for the MDR samples. The red circles in both figures specify the spectral positions of the numerically obtained resonances under study with metasurfaces over the glass without ITO, while the central wavelength of the ENZ mode (~ 1460 nm), derived from the wave equation in the ITO layer, as explained in the Supporting Information, is demonstrated with solid lines. For the hybridized modes, the polariton branches are observable in Figure 2 as transmittance dips. While the upper polariton is clearly visible, the lower polariton dip in transmission is more subtle.

The white circles in Figures 2a and b represent the analytically obtained resonance positions, as explained in section 1 of the Supporting Information. We use Δf as a fitting parameter in our analytical model to minimize the deviation of the upper and lower polariton branches between the numerical simulation and analytical results. This value of Δf is equal to the spectral separation of hybrid modes at the dimension at which they are nearest to each other. We find that $\Delta f = 21$ THz for the EDR case and $\Delta f = 26$ THz for the MDR case. Comparing the magnitude of this anticrossing with the line widths of the resonances in the absence of ITO (around 12 THz) shows that the degree of anticrossing is significantly larger than the line widths of either Mie resonance in the absence of ITO, suggesting a strong coupling between those resonances and the ENZ mode. We note that this simple strong coupling theory describes the coupling of each Mie mode to the ENZ mode in a geometrically complex system. According to eq 1 of the Supporting Information, the ENZ mode's central frequency depends on the superstrate's

permittivity. In our case, the effective permittivity of the metasurface superstrate undergoes significant modification due to the antennas and their resonant conditions. Covering over 40% of the surface area and possessing substantial refractive indices, combined with non-negligible thicknesses, these antennas substantially alter the central frequency of the ENZ mode. That can explain the slight deviations in the analytical results from the simulation.

The details of the fabrication process are explained in section 2 of the Supporting Information. Figure 3a shows an SEM image of one of the fabricated devices. The samples were characterized in a wide-band linear measurement setup where a polarized uncollimated white light was focused on the samples and then recollimated to measure the transmittance of the metasurfaces on ITO. Figures 3b and c show the simulated and experimental transmittances of representative EDR and MDR samples, respectively. We observe a very good agreement between the experimental and simulation data in the magnitude of the anticrossings and the depth of the upper polariton branch, although there are some minor deviations in the resonance wavelengths and the transmittance. The deviations mostly arise from the uncertainty in the thickness of ITO at different locations of the samples. During fabrication, the dry etching process may have partially removed ITO from the exposed spaces between nanoantennas. Fabrication variations in the dimensions of the antennas could be another reason for deviations.

Figures 4a and b show the simulation and experimental results of the resonant wavelengths of different resonances as a function of dimensions. We extracted the position of the polariton branches in the experiment from the transmittance for each sample, as indicated by points in Figure 4a for the EDR case and Figure 4b for the MDR case. We observe a good agreement between the simulation and experiment for the EDR and MDR cases.

We have shown with simulations, analytical modeling, and experimental characterization that the two fundamental Mie modes of an a-Si metasurface, EDR and MDR, can strongly couple to the ENZ mode of a 23 nm layer of ITO. The main evidence for the strong coupling between the modes above is the avoided crossing of the hybrid modes of the metasurface over ITO that is larger than the line widths of the Mie modes

in the absence of ITO. The strength of the coupling and the depth of the resonances related to the hybrid modes could be further strengthened by using slightly thicker ITO layers to reduce the modal volume mismatch between the ENZ mode and the Mie modes.

Plasmonic metasurfaces that are strongly coupled to an ENZ mode of a TCO substrate have been shown to strongly enhance the nonlinear optical response of the ENZ material and thus create the opportunity for engineering dynamic, highly nonlinear metasurfaces.^{33,37,38} As a proof of principle for using the strongly coupled Mie–ENZ hybridized modes shown here in nonlinear applications, we performed degenerate pump–probe experiments, sketched schematically in Figure 5a, using 120 fs pulses. The pump pulses trigger a

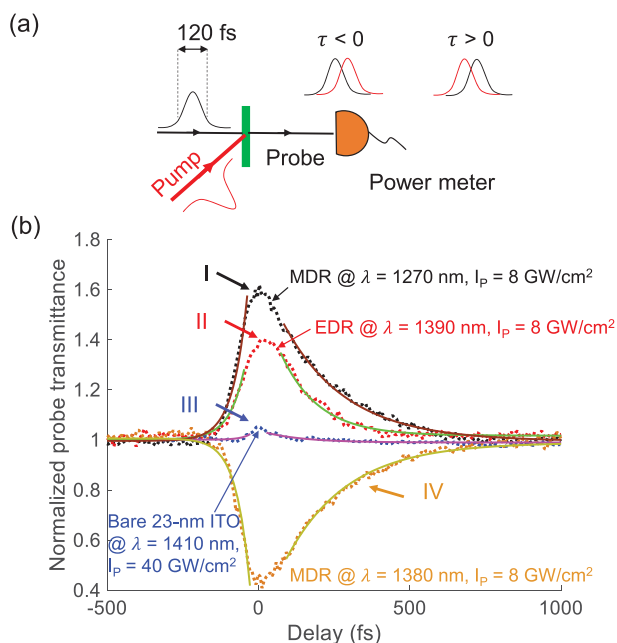


Figure 5. Nonlinear behavior of the samples. (a) A simple schematic of the time-resolving degenerate nonlinear measurement setup. An intense femtosecond (fs) pump beam triggers the nonlinear response of the sample, while a probe beam of the same duration interacts with the modified medium. (b) Normalized transmittance of the probe. The dotted lines show the normalized transmittance of a probe beam of light plotted with respect to the time delay between the pump and the probe for a bare 23 nm-thick ITO sample (in blue, curve III), one of the arrays in the EDR sample (in red, curve II), and one of the arrays in MDR sample at different incident wavelengths (1270 nm in black, curve I, and 1380 nm in brown, curve IV). Negative time delays mean that the probe precedes the pump at the sample. The solid curves represent the fitting results of the rising and falling edges of each curve to exponential equations to derive the rise and fall times of the induced nonlinear change in transmission. Curves I–IV exhibit rise times of 35, 49, 47, and -46 fs, and the slower relaxation times are 132, 130, 205, and 200 fs, respectively.

nonlinear response of the coupled sample of nanoantennas and ITO substrate similar to the plasmonic nanoantennas over ITO, which is then characterized by the transmittance of the weaker probe pulse at different relative timings to the pump.^{33,37} Note that the role of antennas is crucial here both because they confine more light into the ITO layer, as can be seen in Figure 1, and also because they allow for the light to couple from free space to the ENZ mode of the ITO layer.²⁴ In the presence of a strong pump, the coupling coefficients

between the Mie and ENZ modes are significantly perturbed due to the strong nonlinear optical response of the ITO substrate. As a consequence of the unity-order change in the refractive index of ITO, the spectral position and the strength of the hybrid modes also change as a function of the pump intensity, further enhancing the overall nonlinear response of the coupled system. Under such circumstances, the transmittance of a probe beam that travels through the sample may increase or decrease depending on the sign of frequency detuning, with respect to the resonant frequencies of the strongly coupled hybrid modes. The experimental results of the pump–probe measurements obtained from our samples are shown in Figure 5b. We recorded the change in transmittance of the frequency-degenerate probe as a function of the pump–probe delay and the pump–probe wavelengths. Figure 5b also shows results obtained in the same pump–probe setup for a bare 23 nm ITO sample. All of the metasurfaces show stronger modification (up to 20 times) in the transmitted power of the probe compared to what can be achieved for the bare 23 nm ITO sample, despite the metasurfaces being pumped with one-fifth the intensity used to pump the bare ITO sample. Thus, we measured a roughly 100-fold enhancement of the probe transmittance modulation in the metasurface. Such strong enhancement reinforces the notion that the metasurfaces achieve a stronger nonlinear response by enabling efficient coupling to the ENZ mode, enhancing the fields therein, and by time-varying changes in the resonant responses of the antennas due to nonlinear changes in ITO. We derived the rise and fall times of the induced nonlinear changes in transmission responses by fitting exponential equations to the experimentally obtained points (solid lines in Figure 5). We found that the rise time can be as short as 35 fs and the fall time can be as long as 205 fs.

The pump–probe responses of the MDR sample specifically show much richer dynamics than those observed for the EDR one. We measured both positive and negative changes in the probe transmittance, depending on the sign of the spectral detuning of the laser frequency from the MDR resonance. This richer response can be attributed to the stronger coupling of the MDR to the ENZ mode. A transmittance modulation of the same order of magnitude as in our case was reported using plasmonic metasurfaces over ITO.³³ However, the multi-resonant and collective natures of dielectric antennas allow the possibility of designing versatile, dynamic all-optical systems by engineering the interactions of each type of Mie mode with ENZ mode separately.³⁹ A comprehensive investigation of the nonlinear responses of these samples is beyond the scope of this work and is the subject of future research. We note that the speed of modification of the transmittance in our strongly coupled system of a-Si and ITO is at least one order of magnitude higher than the previously reported modification speeds of systems based on bare silicon.^{40,41} In addition, the nonlinear response of the Si-ENZ-based metasurfaces can be further enhanced by using ITO layers of critical thickness.⁴² The nonlinear response of an array of dielectric metasurface on a 33 nm ITO, where the EDR and the MDR both spectrally overlap at the ENZ region of the ITO layer, has been recently reported.⁴³ However, their discussion lacks the details of the role of each type of resonance in the modifications of the linear and nonlinear responses separately. The complete understanding of nonlinear dynamics of individual coupled Mie–ENZ resonances is essential for designing systems that exhibit richer spatiotemporal responses, for example, a time-varying

gradient metasurface that exploits the interactions of a group of Mie modes with a thin ENZ substrate.

In conclusion, we designed, simulated, fabricated, and tested a system to demonstrate strong coupling between the fundamental EDR and MDR Mie modes in an a-Si metasurface to the ENZ mode of a thin layer of ITO. Clear agreement among analytical, simulation, and experimental results confirmed that strong coupling of individual Mie resonances to the ENZ mode could be achieved, eliminating the concern that Mie resonances would have insufficient mode overlap with the ENZ mode to do so. Furthermore, we performed pump–probe nonlinear measurements that showed at least a 100-fold enhancement of transmission modulation through the metasurface in comparison to the already highly nonlinear bare ITO. The metasurface also seems to alter the subpicosecond onset and relaxation times of this modulation, although this relationship merits further investigation. Such coupled metasurface systems could be used for many applications requiring highly nonlinear responses with subpicosecond temporal modulation. While this was already known for plasmonic metasurfaces,^{33,37,38} the option for doing so with dielectric nanoantennas significantly expands the fabrication options. Potentially, even more importantly, it enables dynamically modulated coupling to higher-quality factor resonances and magnetic dipole modes.

■ ASSOCIATED CONTENT

SI Supporting Information

The Supporting Information is available free of charge at <https://pubs.acs.org/doi/10.1021/acs.nanolett.3c03301>.

The initial section provides an in-depth exploration of the analytical formulation of the ENZ mode and the spectral placement of hybrid modes within a coupled system; the second section delves into the intricacies of device fabrication (PDF)

■ AUTHOR INFORMATION

Corresponding Authors

Mohammad Karimi – Department of Electrical and Computer Engineering, University of Ottawa, Ottawa, ON, Canada K1N 6N5; orcid.org/0000-0002-2923-5984; Email: karimimohammad1991@gmail.com

M. Zahirul Alam – Department of Physics, University of Ottawa, Ottawa, ON, Canada K1N 6N5; Email: zahirul.alam@gmail.com

Authors

Kashif Masud Awan – Institute of Materials Science and Engineering, Washington University in Saint Louis, St. Louis, Missouri 63130, United States

Yaswant Vaddi – Department of Physics, University of Ottawa, Ottawa, ON, Canada K1N 6N5

Rasoul Alaei – Institute of Theoretical Solid State Physics, Karlsruhe Institute of Technology, 76131 Karlsruhe, Germany; orcid.org/0000-0003-2187-4949

Jeremy Upham – Department of Physics, University of Ottawa, Ottawa, ON, Canada K1N 6N5

Robert W. Boyd – Department of Physics, University of Ottawa, Ottawa, ON, Canada K1N 6N5; Institute of Optics, University of Rochester, Rochester, New York 14620, United States; orcid.org/0000-0002-1234-2265

Complete contact information is available at:

<https://pubs.acs.org/10.1021/acs.nanolett.3c03301>

Notes

The authors declare no competing financial interest.

■ ACKNOWLEDGMENTS

This work was supported by the Natural Sciences and Engineering Research Council of Canada under Discovery Grant RGPIN/2017-06880, the Canada Research Chairs program under award 950-231657, and the Canada First Research Excellence Fund on Transformative Quantum Technologies under award 072623. R.W.B. acknowledges the US Office of Naval Research award N00014-19-1-2247 and MURI award N00014-20-1-2558. R.A. acknowledges the support of the Alexander von Humboldt Foundation through the Feodor Lynen Fellowship. We acknowledge the support of Stewart Blusson Quantum Matter Institute and the use of their Advanced Nanofab Facility for the fabrication of the samples. K.M.A. acknowledges funding from SiEPIC fab for the fabrication of the devices.

■ REFERENCES

- (1) Jahani, S.; Jacob, Z. All-dielectric metamaterials. *Nature Nanotechnol.* **2016**, *11*, 23–36.
- (2) Xiong, C.; Bell, B.; Eggleton, B. J. CMOS-compatible photonic devices for single-photon generation. *Nanophotonics* **2016**, *5*, 427–439.
- (3) Liu, T.; Xu, R.; Yu, P.; Wang, Z.; Takahara, J. Multipole and multimode engineering in Mie resonance-based metastructures. *Nanophotonics* **2020**, *9*, 1115–1137.
- (4) Azzam, S. I.; Kildishev, A. V. Photonic bound states in the continuum: from basics to applications. *Advanced Optical Materials* **2021**, *9*, No. 2001469.
- (5) Tian, J.; Li, Q.; Belov, P. A.; Sinha, R. K.; Qian, W.; Qiu, M. High-Q all-dielectric metasurface: super and suppressed optical absorption. *ACS Photonics* **2020**, *7*, 1436–1443.
- (6) Kuznetsov, A. I.; Miroshnichenko, A. E.; Brongersma, M. L.; Kivshar, Y. S.; Luk'yanchuk, B. Optically resonant dielectric nanostructures. *Science* **2016**, *354*, No. aag2472.
- (7) Chong, K. E.; Wang, L.; Staude, I.; James, A. R.; Dominguez, J.; Liu, S.; Subramania, G. S.; Decker, M.; Neshev, D. N.; Brener, I.; et al. Efficient polarization-insensitive complex wavefront control using Huygens' metasurfaces based on dielectric resonant meta-atoms. *ACS Photonics* **2016**, *3*, 514–519.
- (8) Rahimzadegan, A.; Arslan, D.; Dams, D.; Groner, A.; Garcia-Santiago, X.; Alaei, R.; Fernandez-Corbaton, I.; Pertsch, T.; Staude, I.; Rockstuhl, C. Beyond dipolar Huygens' metasurfaces for full-phase coverage and unity transmittance. *Nanophotonics* **2020**, *9*, 75–82.
- (9) Yang, Q.; Kruk, S.; Xu, Y.; Wang, Q.; Srivastava, Y. K.; Koshelev, K.; Kravchenko, I.; Singh, R.; Han, J.; Kivshar, Y.; et al. Mie-Resonant Membrane Huygens' Metasurfaces. *Adv. Funct. Mater.* **2020**, *30*, No. 1906851.
- (10) Alaei, R.; Filter, R.; Lehr, D.; Lederer, F.; Rockstuhl, C. A generalized Kerker condition for highly directive nanoantennas. *Optics Letters* **2015**, *40*, 2645–2648.
- (11) Liu, W.; Kivshar, Y. S. Generalized Kerker effects in nanophotonics and meta-optics. *Opt. Express* **2018**, *26*, 13085–13105.
- (12) Hwang, M.-S.; Lee, H.-C.; Kim, K.-H.; Jeong, K.-Y.; Kwon, S.-H.; Koshelev, K.; Kivshar, Y.; Park, H.-G. Ultralow-threshold laser using super-bound states in the continuum. *Nat. Commun.* **2021**, *12*, 4135.
- (13) Huang, C.; Zhang, C.; Xiao, S.; Wang, Y.; Fan, Y.; Liu, Y.; Zhang, N.; Qu, G.; Ji, H.; Han, J.; et al. Ultrafast control of vortex microlasers. *Science* **2020**, *367*, 1018–1021.
- (14) Tuz, V. R.; Khardikov, V. V.; Kivshar, Y. S. All-dielectric resonant metasurfaces with a strong toroidal response. *ACS Photonics* **2018**, *5*, 1871–1876.

- (15) Kivshar, Y. All-dielectric meta-optics and non-linear nanophotonics. *National Science Review* **2018**, *5*, 144–158.
- (16) Kruk, S.; Kivshar, Y. Functional meta-optics and nanophotonics governed by Mie resonances. *ACS Photonics* **2017**, *4*, 2638–2649.
- (17) Zograf, G.; Zalogina, A.; Koshelev, K.; Choi, D.-Y.; Korolev, V.; Hollinger, R.; Kartashov, D.; Zürich, M.; Spielmann, C.; Makarov, S.; et al. High-harmonic generation in dielectric metasurfaces empowered by bound states in the continuum. *2020 Conference on Lasers and Electro-Optics (CLEO)* **2020**, 1–2.
- (18) Shcherbakov, M. R.; Liu, S.; Zubyuk, V. V.; Vaskin, A.; Vabishchevich, P. P.; Keeler, G.; Pertsch, T.; Dolgova, T. V.; Staude, I.; Brener, I.; et al. Ultrafast all-optical tuning of direct-gap semiconductor metasurfaces. *Nat. Commun.* **2017**, *8*, 1–6.
- (19) Koshelev, K.; Kruk, S.; Melik-Gaykazyan, E.; Choi, J.-H.; Bogdanov, A.; Park, H.-G.; Kivshar, Y. Subwavelength dielectric resonators for nonlinear nanophotonics. *Science* **2020**, *367*, 288–292.
- (20) Bohn, J.; Bucher, T.; Chong, K. E.; Komar, A.; Choi, D.-Y.; Neshev, D. N.; Kivshar, Y. S.; Pertsch, T.; Staude, I. Active tuning of spontaneous emission by Mie-resonant dielectric metasurfaces. *Nano Lett.* **2018**, *18*, 3461–3465.
- (21) Forouzmmand, A.; Mosallaei, H. Dynamic beam control via Mie-resonance based phase-change metasurface: a theoretical investigation. *Opt. Express* **2018**, *26*, 17948–17963.
- (22) Vaskin, A.; Mashhadi, S.; Steinert, M.; Chong, K. E.; Keene, D.; Nanz, S.; Abass, A.; Rusak, E.; Choi, D.-Y.; Fernandez-Corbaton, I.; et al. Manipulation of magnetic dipole emission from Eu³⁺ with Mie-resonant dielectric metasurfaces. *Nano Lett.* **2019**, *19*, 1015–1022.
- (23) Reshef, O.; De Leon, I.; Alam, M. Z.; Boyd, R. W. Nonlinear optical effects in epsilon-near-zero media. *Nature Reviews Materials* **2019**, *4*, 535–551.
- (24) Alam, M. Z.; De Leon, I.; Boyd, R. W. Large optical nonlinearity of indium tin oxide in its epsilon-near-zero region. *Science* **2016**, *352*, 795–797.
- (25) Vezzoli, S.; Bruno, V.; DeVault, C.; Roger, T.; Shalaev, V. M.; Boltasseva, A.; Ferrera, M.; Clerici, M.; Dubietis, A.; Faccio, D. Optical time reversal from time-dependent epsilon-near-zero media. *Physical review letters* **2018**, *120*, No. 043902.
- (26) Vassant, S.; Hugonin, J.-P.; Marquier, F.; Greffet, J.-J. Berreman mode and epsilon near zero mode. *Opt. Express* **2012**, *20*, 23971–23977.
- (27) Campione, S.; Wendt, J. R.; Keeler, G. A.; Luk, T. S. Near-infrared strong coupling between metamaterials and epsilon-near-zero modes in degenerately doped semiconductor nanolayers. *ACS Photonics* **2016**, *3*, 293–297.
- (28) Schulz, S. A.; Tahir, A. A.; Alam, M. Z.; Upham, J.; De Leon, I.; Boyd, R. W. Optical response of dipole antennas on an epsilon-near-zero substrate. *Phys. Rev. A* **2016**, *93*, No. 063846.
- (29) Jun, Y. C.; Reno, J.; Ribaudo, T.; Shaner, E.; Greffet, J.-J.; Vassant, S.; Marquier, F.; Sinclair, M.; Brener, I. Epsilon-near-zero strong coupling in metamaterial-semiconductor hybrid structures. *Nano Lett.* **2013**, *13*, 5391–5396.
- (30) Passler, N. C.; Gubbin, C. R.; Folland, T. G.; Razdolski, I.; Katzer, D. S.; Storm, D. F.; Wolf, M.; De Liberato, S.; Caldwell, J. D.; Paarmann, A. Strong coupling of epsilon-near-zero phonon polaritons in polar dielectric heterostructures. *Nano Lett.* **2018**, *18*, 4285–4292.
- (31) Tong, J.; Suo, F.; Tobing, L. Y.; Yao, N.; Zhang, D.; Huang, Z.; Zhang, D. H. High order magnetic and electric resonant modes of split ring resonator metasurface arrays for strong enhancement of mid-infrared photodetection. *ACS Appl. Mater. Interfaces* **2020**, *12*, 8835–8844.
- (32) Shalaev, M. I.; Sun, J.; Tsukernik, A.; Pandey, A.; Nikolskiy, K.; Litchinitser, N. M. High-efficiency all-dielectric metasurfaces for ultracompact beam manipulation in transmission mode. *Nano Lett.* **2015**, *15*, 6261–6266.
- (33) Alam, M. Z.; Schulz, S. A.; Upham, J.; De Leon, I.; Boyd, R. W. Large optical nonlinearity of nanoantennas coupled to an epsilon-near-zero material. *Nat. Photonics* **2018**, *12*, 79–83.
- (34) Alaei, R.; Vaddi, Y.; Boyd, R. W. Dynamic coherent perfect absorption in nonlinear metasurfaces. *Opt. Lett.* **2020**, *45*, 6414–6417.
- (35) Novotny, L. Strong coupling, energy splitting, and level crossings: A classical perspective. *American Journal of Physics* **2010**, *78*, 1199–1202.
- (36) Staude, I.; Miroshnichenko, A. E.; Decker, M.; Fofang, N. T.; Liu, S.; Gonzales, E.; Dominguez, J.; Luk, T. S.; Neshev, D. N.; Brener, I.; et al. Tailoring directional scattering through magnetic and electric resonances in subwavelength silicon nanodisks. *ACS Nano* **2013**, *7*, 7824–7832.
- (37) Karimi, M.; Alam, M. Z.; Upham, J.; Reshef, O.; Boyd, R. W. Time-varying gradient metasurface with applications in all-optical beam steering. *Nanophotonics* **2023**, *12*, 1733–1740.
- (38) Bruno, V.; DeVault, C.; Vezzoli, S.; Kudyshev, Z.; Huq, T.; Mignuzzi, S.; Jacassi, A.; Saha, S.; Shah, Y. D.; Maier, S. A.; et al. Negative refraction in time-varying strongly coupled plasmonic-antenna-epsilon-near-zero systems. *Physical review letters* **2020**, *124*, No. 043902.
- (39) Zhou, Y.; Guo, S.; Overvig, A. C.; Alù, A. Multiresonant Nonlocal Metasurfaces. *Nano Lett.* **2023**, *23*, 6768–6875.
- (40) Almeida, V. R.; Barrios, C. A.; Panepucci, R. R.; Lipson, M. All-optical control of light on a silicon chip. *Nature* **2004**, *431*, 1081–1084.
- (41) Upham, J.; Tanaka, Y.; Asano, T.; Noda, S. On-the-fly wavelength conversion of photons by dynamic control of photonic waveguides. *Applied physics express* **2010**, *3*, No. 062001.
- (42) Choudhary, S.; Iqbal, S.; Karimi, M.; Reshef, O.; Alam, M. Z.; Boyd, R. W. Strongly Coupled Plasmon Polaritons in Gold and Epsilon-Near-Zero Bilayers. *ACS photonics* **2023**, *10*, 162–169.
- (43) Wang, K.; Liu, A.-Y.; Hsiao, H.-H.; Genet, C.; Ebbesen, T. Large Optical Nonlinearity of Dielectric Nanocavity-Assisted Mie Resonances Strongly Coupled to an Epsilon-near-Zero Mode. *Nano Lett.* **2022**, *22*, 702–709.

Supplementary Information

Interactions of fundamental Mie modes with thin epsilon-near-zero substrates

Mohammad Karimi,^{*,†} Kashif Masud Awan,[‡] Yaswant Vaddi,[†] Rasoul Alaei,[¶]
Jeremy Upham,[§] M. Zahirul Alam,^{*,§} and Robert W. Boyd^{§,||}

[†]*Department of Electrical and Computer Engineering, University of Ottawa, Ottawa, ON,
Canada, K1N 6N5*

[‡]*Institute of Materials Science and Engineering, Washington University in Saint Louis,
St.Louis, MO 63130, USA*

[¶]*Institute of Theoretical Solid State Physics, Karlsruhe Institute of Technology,
Wolfgang-Gaede-Str.1, 76131, Karlsruhe, Germany*

[§]*Department of Physics, University of Ottawa, Ottawa, ON, Canada, K1N 6N5*

^{||}*Institute of Optics, University of Rochester, 275 Hutchison Rd Wilmot Bldg, Rochester,
NY 14620, USA*

E-mail: karimimohammad1991@gmail.com; zahirul.alam@gmail.com

Abstract

This document contains the supplemental information for the letter entitled "Interactions of fundamental Mie modes with thin epsilon-near-zero substrates". Section S1 presents the theoretical model used for fitting the data to the simulation results and extracting the frequency detunings due to the strong coupling effect. Section S2 provides information about the fabrication of the samples.

S1. Analytical Modeling

In our analytical model, the central wavelength of the ENZ mode was derived by solving the following dispersion relation of the modes in a thin layer of material with a permittivity of ε_1 sandwiched between two layers of permittivities ε_0 and ε_2 ¹ :

$$1 + \frac{\varepsilon_0 k_{z2}}{\varepsilon_2 k_{z0}} = i \tan(k_{z1} d) \left(\frac{\varepsilon_1 k_{z2}}{\varepsilon_2 k_{z1}} + \frac{\varepsilon_0 k_{z1}}{\varepsilon_1 k_{z0}} \right) \quad (1)$$

where $k_{zi}^2 = \varepsilon_i \frac{\omega^2}{c^2} - k_{\parallel}^2$, k_{\parallel} is the transverse wavenumber; ω is the angular frequency; d is the thickness of the middle layer; and c is the speed of light in vacuum. To solve these equations, we used the permittivity of ITO derived from the ellipsometry data. We found that the central wavelength of the ENZ mode is around 1460 nm. Note that this wavelength is different from the point where the real part of permittivity vanishes, although they are near each other.

To analyze the strongly coupled system, we used the theory explained in previous works.^{2,3} According to this model, the frequencies of the lower and upper branches after the coupling can be calculated as a function of the isolated resonance frequencies using the following relations:

$$\omega_{\pm} = \frac{1}{2} (\omega_{\text{DR}} + \omega_{\text{ENZ}} \pm \sqrt{(\omega_{\text{DR}} - \omega_{\text{ENZ}})^2 + 4\Delta^2}) \quad (2)$$

where $\Delta = 2\pi\Delta f$ is the angular frequency difference between the split modes; ω_+ and ω_- are the frequencies of the hybrid modes of upper and lower polariton branches, respectively; and ω_{DR} and ω_{ENZ} are the resonance frequencies for the dipole resonances and the ENZ mode, respectively. The white circles in Figures 2(a) and 2(b) in the main text represent the analytically obtained resonances. We use Δf as a fitting parameter in our analytical model to minimize the deviation of the upper and lower polariton branches between the numerical simulation and the analytical results. This value of Δf is equal to the spectral separation of hybrid modes at the dimension that they are nearest to each other.

S2. Fabrication Process

We fabricated structures with different antennas/lattice dimensions to study the coupling of the EDR/MDR to the ENZ mode. A 23 nm-thick ITO on SiO₂ samples was obtained from a commercial source. The ITO samples were cleaned, followed by deposition of 230 nm a-Si via PECVD at 1000 mT, 210 oC with an RF power of 10 W using 25 sccm Silane and 475 sccm of Argon. To pattern the metasurface into the a-Si layer, a spin-coat of 500 nm Zep-520a (a positive-tone EBL resist) was hard baked at 180 oC for 2 min, then was exposed using a 100 keV EBL system with a dosage of 210 $\mu\text{C}/\text{cm}^2$ followed by development in N-Amyl Acetate for 1 min. The pattern is then transferred into the a-Si layer by ICP-RIE a pressure of 10 mT, temperature of 20 oC, ICP power of 100 W, and RIE power of 20 W with 30 sccm of C₄F₈ and 20 sccm of SF₆. Residual Zep resist was then removed using acetone before inspection of the samples using optical and electron microscopes. Figure 3(a) in the main text shows the SEM image of one of the fabricated devices.

References

- (1) Vassant, S.; Hugonin, J.-P.; Marquier, F.; Greffet, J.-J. Berreman mode and epsilon near zero mode. *Optics express* **2012**, *20*, 23971–23977.
- (2) Novotny, L. Strong coupling, energy splitting, and level crossings: A classical perspective. *American Journal of Physics* **2010**, *78*, 1199–1202.
- (3) Bruno, V.; DeVault, C.; Vezzoli, S.; Kudyshev, Z.; Huq, T.; Mignuzzi, S.; Jacassi, A.; Saha, S.; Shah, Y. D.; Maier, S. A.; others Negative refraction in time-varying strongly coupled plasmonic-antenna-epsilon-near-zero systems. *Physical review letters* **2020**, *124*, 043902.